Conversion of greenhouse gases to synthetic fuel using a sustainable cyclic plasma process

M. M. Sarafraz, F. C. Christo, Nam Tran, L. Fulcheri, V. Hessel

School of Engineering, Deakin University, Waurn Ponds Campus, Geelong, VIC.

[*Corresponding author]

Email: Mohsen.sarafraz@deakin.edu.au

Tel: +61416311335

Abstract

In the present article, a new thermodynamic process is proposed in which a thermal plasma reactor is utilised to dissociate carbon dioxide/steam blend into synthetic fuel using chemical looping technology. Chrome/chrome oxide (Cr/Cr_2O_3) pair was used as the oxygen carrier and also the thermal transport medium between the thermal plasma reactor and a synthetic fuel fluidized bed reactor. The proposed process was hybridised with renewable energy resources including solar photovoltaic and wind to account for the energy demand of the thermal plasma reactor. Results showed that at a molar ratio of CO_2/Cr = 1.12 and steam/Cr ratio = 2.8, the syngas quality referred to as H_2: CO > 2.05, which is suitable for liquid fuel production and Fischer-Tropsch applications. Also, the thermal plasma reactor reached chemical conversion >0.99 at 5273 K, while SFR represented the conversion extent >0.95 at 1473 K. The highest thermodynamic efficiency of the proposed process was 0.43 with a 3 MW electricity production capacity that could be utilised by thermal plasma aiming at improving self-sustaining factor of the system. The integration of the system with solar photovoltaic and wind in Whyalla, South Australia, showed that the renewable energy penetration in the proposed system can be as high as 68.4% with battery storage of 30 MWh together with an installed capacity of 50 MW and 37.5 MW for photovoltaic panels and wind turbines, respectively. Larger battery storage did not affect the renewable energy fraction as solar irradiance and wind velocity were not sufficient to complete the charging cycle of the battery.

Keywords: Synthetic fuel; hydrogen; renewable energy; thermal plasma; chromium particle.

1. Introduction

With population growth and the improvement of living standards of developing communities, the need to secure energy has surged across the world. Currently, fossil fuels account for 84% of the world energy [1] and are forecasted to remain the main source of energy for the next two decades [2]. Combustion of fossil fuels is a well-established technology for utilising energy from carbon-containing fuels, which is also the dominant CO_2 emission source into the atmosphere. Carbon dioxide has been recognised as a key greenhouse gas, which is directly linked to global warming. By increasing the atmosphere temperature, as becoming evident in Australia [3], natural disasters such as storms, floods, and local droughts are intensified threatening the fate of humans, animals, and the planet's ecosystem.

In the IPCC report [4] and Paris Summit [5], the focus is shifting towards suppressing the effect of greenhouse gases on the environment by decarbonisation of the industry, while at the same time seeking alternative energy resources, developing new technologies to reduce and/or eliminate the production of GHGs, in particular, CO_2 [6].

Improving existing fossil-based combustion systems, developing new energy technologies, hybridised systems with renewable energy or bio-derived clean energy resources, such as biomass [7], are potential pathways that contribute to the mitigation of global warming. Solar photovoltaic (PV) and wind energy are two mature renewable energy resources that are currently being deployed either as stand-alone systems or through integration with conventional industrial plants, and commercial and domestic sectors [8]. According to Annual Technology Baseline 2021 by NREL [9], Photovoltaic panels (with an efficiency of >25%) are projected to provide a competitive Levelized cost of energy (LCOE) of 18 $/MWh by 2030, while wind energy's LCOE is expected to be 36 $/MWh by that date. Capitalising on these technologies as green energy sources offer an opportunity to integrate them with new technologies to further reduce the emission of CO_2 and other GHGs from conventional combustion systems into the atmosphere.

In parallel to adopting renewable energy systems, especially during the transition phase towards carbon-free energy sources, the decarbonisation process should also include technologies for converting the emitted GHG's into useful fuels. This requires a robust circular economy framework that acts as an enabler platform for developing clean processes [10]. Such processes can absorb and convert GHGs into cleaner fuels without further emission of GHGs. Synthetic fuel (a mixture of H_2, CO and a small amount of CH_4) produced from CO_2 is one

potential solution that converts the CO_2 into value-added chemicals. Synthetic fuel can be converted into hydrogen, alcohol, and liquid fuels.

Currently, synthetic fuel is primarily produced by steam or air gasification [11] or dual bed gasification of feedstock and carbon-containing resources, which are inherently associated with the emission of CO_2 into the atmosphere. Also, current gasification technologies are driven by hydrothermal gasification reaction, Boudouard reaction mixed with water gas shift reaction. Thus, these gasification processes inherently induce CO_2, Particulate Matters such as dust, dirt, soot, or agglomerated solids in smoke (PM2.5) and carbon particles into the atmosphere [12]. Therefore, conventional gasification processes are not sustainable and alternative cleaner processes are needed.

With the advent of Chemical Looping Process (CLP) technology, a new pathway for synthetic fuel production was developed offering higher efficiency and thermal performance, and lower CO_2 production in comparison with conventional air gasification systems. Cyclic reduction of metal oxides in a CLP is one potential pathway to be utilised for hydrogen production or gasification to produce synthetic fuel [13]. A chemical looping system utilises two main reactors. The first reactor is referred to as a "synthetic fuel reactor" in which a metal/metal oxide reacts with carbonaceous feedstock to produce synthetic fuel and a reduced metal. In the second reactor referred to as oxidation or air reactor, the reduced metal is converted to metal oxide using an air-driven reaction. This operation is cyclic meaning that metal will go through successive reduction and oxidation. Synthetic fuel (or hydrogen) is produced in the reduction reactor, while vitiated air is the main product of the oxidation reactor. While conventional CLP is a promising method for producing high-quality synthetic fuel, gasification via CLP is still associated with the production of CO_2 appearing in the synthetic fuel, thereby affecting the quality of the fuel and environment.

In this paper, we propose a series of changes to the conventional CLP process:

(i) The foremost change is to replace the fossil fuel with a blend of gaseous CO_2 and steam that is captured from flue gas of a fossil-fuel combustion plant or can be mixed on-site. This is a gaseous-phase CLP process, hence differs fundamentally from conventional CLP processes that are designed for gasification of solid feedstock or reforming of natural gas.

(ii) The second key modification is the use of chrome oxide particles as an oxygen carrier between reactors. Chrome has favourable mechanical properties such as resistance against

abrasion, agglomeration and sintering. Also, the physical properties of chrome such as thermal conductivity and density are suitable for thermochemical processes;

(iii) The third key change is to utilise a thermal plasma reactor as an enabler to provide high temperatures such as 6000 K to reduce chrome oxide into chrome and oxygen, which cannot be achieved by conventional reactors.

With the above changes, the CLP can be utilised to dissociate CO_2 directly into synthetic fuel without emitting GHGs into the atmosphere. Hence, the overarching aim of this paper is to develop a novel direct CO_2 -to-synthetic fuel chromium-based CPL process, which also integrates renewable energy resources such as PV and wind. Accordingly, the objectives of this research are:

1- To characterise the proposed process for CO_2 dissociation via cyclic reduction and oxidation of chromium oxide/chromium particles.
2- To analyse the thermodynamic potential of the proposed system for integration with renewable energy resources; and
3- To assess the energetic performance of the process including thermodynamic efficiency, self-sustaining factor, and quality of the synthetic fuel produced with the proposed process.

To hybridise the proposed system with renewable energy, a control system was developed for switching between grid power and renewable energy. Also, a heat recovery system was included to recover the parasitic heat loss to generate electricity, which can partially maintain the energy demand of the thermal plasma reactor. The Effect of key operating parameters such as temperature, reactant molar ratios, and dynamic energy parameters, on the performance of the proposed system, were investigated and discussed. Successful integration of solar and wind for supplying the energy demand of the process was demonstrated for the town of Whyalla located in South Australia because of its high solar insolation.

2. Thermal plasma, disruptive technology

The proposed chromium-based CLP system will utilise two reactors, a synthetic fuel reactor (SFR) and a thermal plasma particle regenerator (TPPR) reactor [14]. The former produces the synthetic fuel from carbon dioxide and steam blend, while the TPPR re-generates the metal by

dissociating the metal oxide into pure metal and oxygen. The pure metal can react with the CO_2/steam gas blend in the SFR.

The heat source for the process will be delivered using a plasma reactor. The utilisation of a plasma reactor in gasification and chemical processes has extensively been investigated and demonstrated the potential of integrating thermal plasma with renewable energy for fuel and gas dissociation processes [15, 16]. For example, Fulcheri et al. [17] utilised an arc thermal plasma reactor for cracking natural gas aiming at producing hydrogen as a fuel and carbon black, which can be utilised in agricultural applications and soil improvements. Gonzalez-Aguilar et al. [18] evaluated various phase-phase thermal plasma systems operating at atmospheric pressure to demonstrate the feasibility of thermal plasma for generating carbon nanostructures and to justify the mechanisms involved in producing carbon particles during plasma processes. Haufler et al. [19] and Parker et al. [20] demonstrated Fullerene synthesis via thermal plasma reactor and discussed the role of electrode distance and characteristics on process performance and reported 26 wt% yields for benzene production. Rohani et al. [21] investigated the potential of thermal plasma for generating energy and renewable fuel from waste combustion and biomass feedstock with lower heating value < 20 MJ/kg. They investigated three scenarios including co-combustion of biomass, oxy-combustion and electro-combustion in which thermal plasma (A DC torch) was utilised to promote the energy economy of the process and to demonstrate the effect of gas sheathing on the lifetime of plasma electrodes during gasification/combustion reactions. These selected examples demonstrate the potential of thermal plasma in renewable energy fuel and gas dissociation processes. The thermal characteristics of equilibrium plasma chemistry offers unique thermodynamic features for driving non-conventional reactions (e.g., reactions with positive ΔG or highly endothermic reactions) and hence it is a disruptive technology candidate for producing clean fuel.

A thermal plasma reactor creates near-equilibrium conditions for the species, charges ions, excited species, neutral particles all carried by a neutral background gas (such as argon, xenon, or nitrogen). In a thermal plasma reactor, the temperature of the gaseous species can reach a temperature of ~7,000-10,000 K [22], which is sufficient to drive reactions with relatively large positive Gibbs free energy of reaction (ΔG). The energy for a thermal plasma reactor can be supplied by electricity (AC or DC), which can be from renewable energy resources such as photovoltaic [23] or wind [24]. These characteristics are leveraged by adding a TPPR to the system to dissociate a metal oxide into a reduced pure metal with a high chemical conversion extent, which otherwise cannot be achieved in a conventional reactor.

3. Conceptual design of the process

In this section, process design, the thermodynamic stability of oxygen carrier together with modelling approaches, assumptions and hybridisation strategy are discussed.

3.1.Process design

An illustration of the proposed CLP is represented in Fig. 1. The system consists of three main units; a synthetic fuel reactor (SFR), a thermal plasma particle regenerator (TPPR), and a steam power block to generate electricity from waste heat recovered from the plant. In the SFR, carbon dioxide and steam react with chromium particles (Cr) to dissociate CO_2 and produce H_2-enriched synthetic fuel. Chromium was selected because of the following reasons:

1) Chromium's melting point is high ranging between 2173 K and 2773 K, which is suitable for the required operating SFR and TPPR conditions.
2) The average thermal conductivity of chromium is high (110-115 W/mK), which is higher than copper or iron particles.
3) Chrome has suitable physical properties for thermochemical processes, Its density and heat capacities are 7150 kg/m^3 and 0.45 kJ/kg.K, respectively, resulting in a volumetric heat capacity (ρc_p) of 3.21 MJ/m^3.K. This is a sufficient capacity for sensible heat transfer and chemical storage of energy to sustain the conversion of $Cr \rightarrow Cr_2O_3$.
4) Chromium is a locally-sourced metal from Coobina in Western Australia with a total capacity of 1.5 Mt with the purity of 29.3% (Cr).

In the SFR, oxygen is absorbed from CO_2 by chromium particles to form chrome oxide, while hydrogen and carbon monoxide together with a small amount of methane form a synthetic fuel that exit the reactor. The generated chrome oxide will then be circulated to the TPPR unit, where the thermal plasma dissociates the chrome oxide back into pure chromium and oxygen. Notably, the dissociation of chrome oxide is an endothermic reaction requiring energy to proceed towards the equilibrium, while dissociation of CO_2 and steam in the presence of chromium is an exothermic reaction, thereby sufficient to maintain the temperature of the reactor.

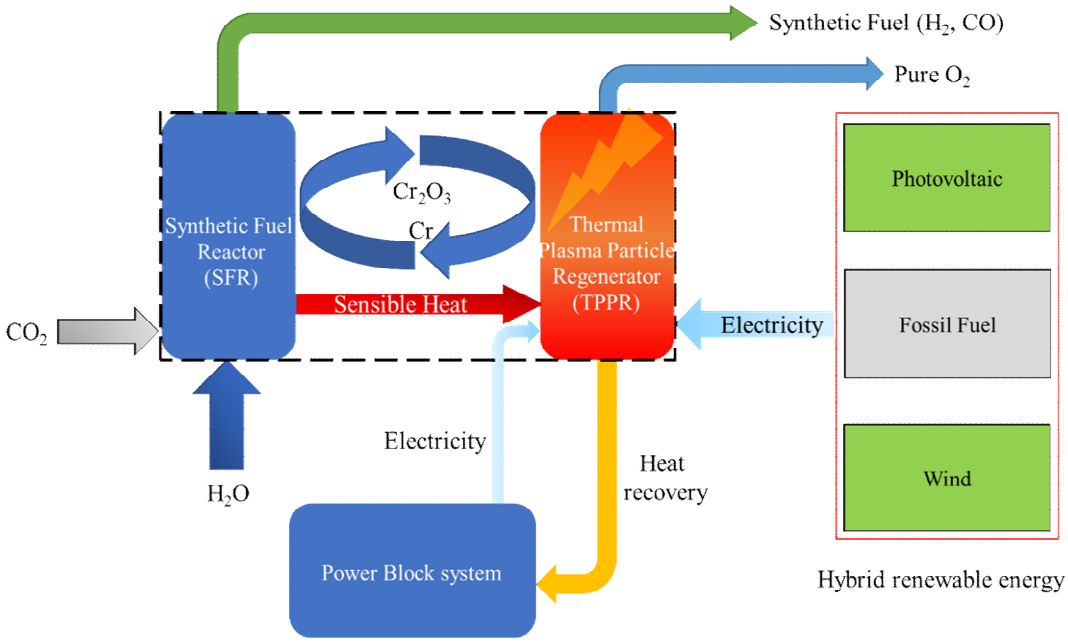

Fig. 1. Schematic diagram of the process developed for synthetic fuel production from CO_2.

The exothermic energy released from the SFR can be carried over to the thermal plasma reactor in the form of sensible thermal energy, hence decreasing the thermal load of the thermal plasma reactor. The heat recovered from the synthetic fuel, oxygen and the exothermic reactor is used to generate steam at 773 K (± 20 K as a design pinch point) at 60 bars. The generated steam is used to produce electricity using a steam turbine to partially cover the electricity demand of the pumps, compressors, and TPPR. To harness renewable energy together with any electricity produced from heat recovery (via steam cycle power block), a control strategy is required to switch between the energy resources and dampen the fluctuation during the transition from renewable/grid to grid/renewable resources.

3.2.Equilibrium analysis of thermal plasma reactor

The temperature-mole percentage thermodynamic equilibrium plot for the $Cr_2O_3 \rightarrow Cr$ plasma plant is shown in Fig. 2. This diagram is essential to identify the exact operating temperature domain in which pure Cr and oxygen become the main components of the outlet stream of the TPPR. As can be observed, at temperature borderline $T \geq 5273$ K, Cr (g), O (g) and O_2 (g) together with electrons and positrons mixed in the gas phase are the components of the TPPR reactor. Thus, the TPPR requires a robust high heat flux cooling system (rapid quenching technology) to generate Cr particles and to avoid recombination of oxygen with Cr particles. The quenching system must meet the following thermodynamic conditions:

(i) It must be constructed from materials that can sustain in harsh environments such as high-temperature and high-pressure (HTHP) operating conditions.

(ii) The quenching system must have sufficient resistance against erosion and corrosion due to the sublimation and condensation of metal vapours on the metallic parts.

(iii) It will also require a specific heat transfer fluid that can remove a high amount of heat without any phase change during the cooling cycle.

It is acknowledged that thermal plasma technology has not been commercialised for metal particle generation. However, its ability to generate carbon particles from gaseous reactants has already been demonstrated. Hence, the technology readiness level will be promoted in the coming years and TPPR will be equipped with rapid quenching technologies suitable for metal particle generation. Overall, temperatures T < 2273 K, are identified as suitable operating temperatures for the SFR, while T > 5273 K is suitable for the TPPR (Fig. 2).

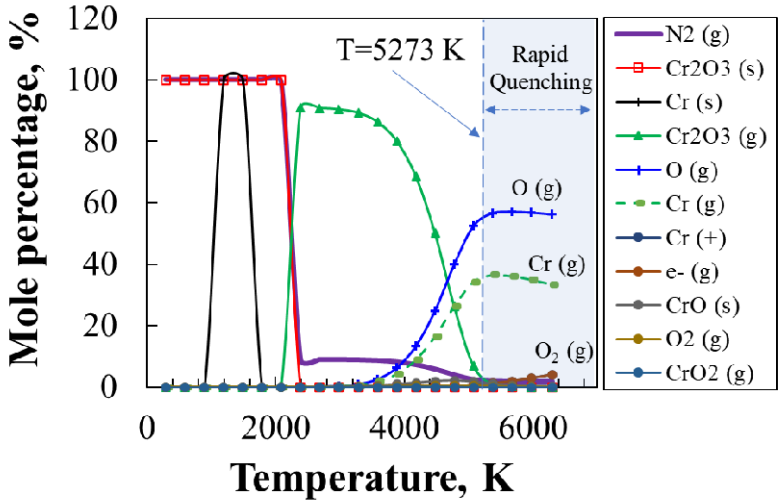

Fig. 2. The calculated variation of the mole percentage of species in a thermal plasma reactor with temperature.

4. Modelling approach

The detailed process flow diagram of the proposed system is shown in Fig. 3a. The inlet (feed) streams to the system are carbon dioxide and steam, and the outlet streams are synthetic fuel from SFR and oxygen from the TPPR. The CO_2 line is slightly pressurised to overcome potential pressure drop, backflow and to feed dioxide carbon into the reactor. The steam was

produced using a high-pressure water line that was heated up to 400 K. The temperature of the inlet steam was regulated based on the temperature of the SFR to avoid any sudden quench and condensation at injection points. Separators were utilised after each reactor to ensure no carried-over particles are transferred with the outlet gaseous products. A series of heat recovery heat exchangers were employed to recover heat from hot streams and utilise them in a steam generation unit in the power block. A steam turbine (single-stage, capacity: 5 MWth) with maximum mechanical and isentropic efficiency of 0.95 was used to convert waste heat recovery into steam. The flow rate of water in the power block was calculated using the design spec feature in Aspen Plus. Thus, depending on the operating conditions, the flow rate of the power block was maintained such that the steam temperature at the inlet of the turbine remains at 773 K ± 20K. This temperature avoids the formation of liquid water inside the turbine and maximised the work extracted from the turbine. The electricity produced by the steam cycle power plant is mainly dedicated to the TPPR unit, hence increasing the process efficiency and self-sustaining feature of the plant. Fig. 3b shows the schematic diagram of the process model developed in Aspen Plus. Uniquac thermodynamic package was utilised to calculate thermophysical properties of the streams under dynamic simulation conditions. The plant was simulated over 8766 hours corresponding to annual continuous operation.

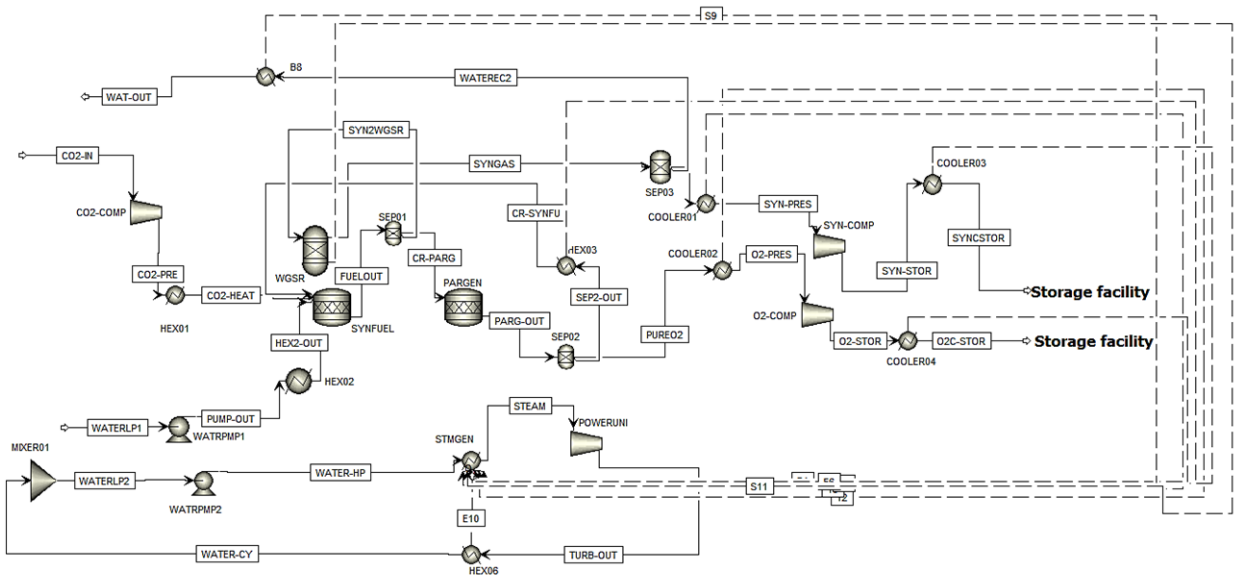

(a)

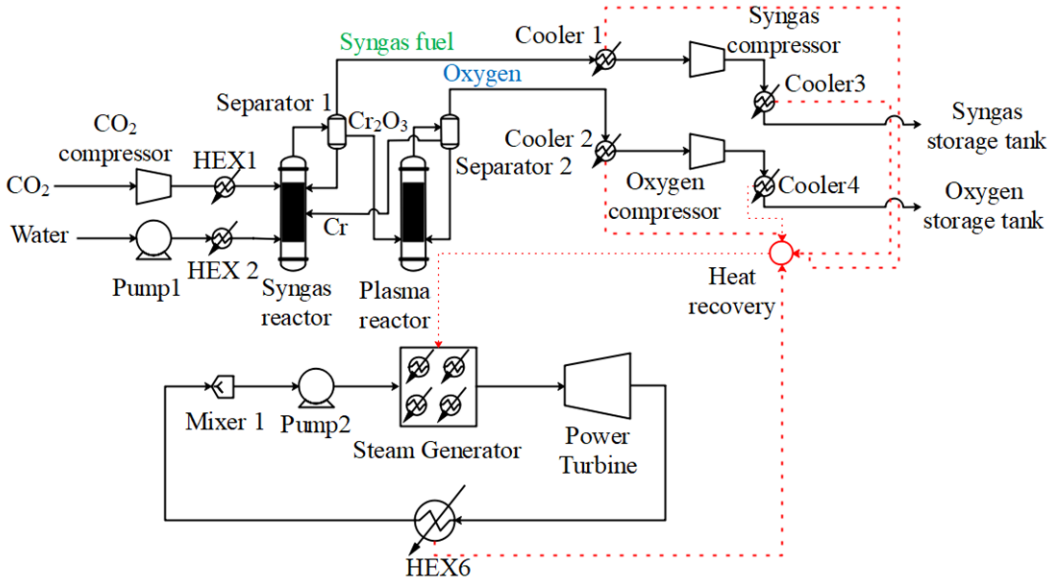

(b)

Fig. 3. (a) An illustration of the process model developed in Aspen Plus together with detailed process flow and streams (b).

To model the whole process, the following assumptions were made and applied:

1- For integrating renewable energy, the process was assumed to operate 8766 hours per year, which is used to assess the hourly energy consumption of the reactors, pumps, compressors, and turbines.
2- Solid-gas reactions proceed towards equilibrium and follow thermochemical equilibrium analysis.
3- Mixers, separators and pumps were assumed to operate at near-ideal conditions.
4- No water is generated and/or accumulated in the steam turbine, thereby the outlet pressure of the turbine was set at > 1 bar and 393 K to prevent water condensation.
5- There is a robust technology available to accumulate and utilise all heat recovery from the system to produce steam in the steam generation unit.
6- There is a robust system developed for circulating chromium particles between reactors at high temperatures. Likewise, it was assumed that steam injection systems are already developed and can distribute steam within the reactor's bed efficiently.
7- There is no heat and mass transfer resistance between particles and reactants (ideal heat and mass transfer).

To estimate thermodynamic parameters including the Gibbs Free Energy (ΔG) and enthalpy of reaction (ΔH), the following equation was used:

$$\Delta z_{R,i} = \sum_{product\ species} \Delta z_i^f - \sum_{reactant\ species} \Delta z_i^f . \quad (1)$$

where Δz_R is either the Gibbs free energy of reaction (ΔG_R) or enthalpy of the reaction (ΔH_R). The subscripts "*i*", refers to species such as CO, H_2, CO_2, CO, CH_4, and H_2O. Likewise, *f* refers to the "formation state" for each thermodynamic property that can be obtained from thermodynamic databases at 298 K. To evaluate the calorific value of the syngas, the following equation was employed:

$$E\chi = \dot{Q}_{syngas} \times (\dot{n}_{H_2} \times LHV_{H_2} + \dot{n}_{CO} \times LHV_{co} + \dot{n}_{CH_4} \times LHV_{cH_4}). \quad (2)$$

Here, $\dot{n}$ is the molar flow rate of the synthetic fuel stream. *LHV* is the lower heating value of the reactive species (~10.1 MJ/kg for CO and ~120 MJ/kg for H_2 and ~50 MJ/kg for CH_4).

The syngas quality (molar ratio of hydrogen to carbon monoxide) was calculated using the following equation:

$$\chi = (\frac{\dot{n}_{H_2}}{\dot{n}_{CO}}). \quad (3)$$

Here, $\dot{n}$ is the molar flow rate of hydrogen and/or CO. The combustion quality was defined as:

$$\chi = (\frac{\dot{n}_{CO_2}}{\dot{n}_{CO}}). \quad (4)$$

Here, $\dot{n}$ is the molar flow rate of CO_2 and CO.

The total thermodynamic efficiency of the process is defined as follows:

$$\eta_{th} = \frac{\sum_{i=1}^{n} n_i \times \Delta H_i]_{out} - Q_{HEX,p} + W_{power\ block} - W_{pump} - W_{compressor} - Q_{loss}}{\sum Q_{net,R_Z} + \sum_{i=1}^{n} n_i \times \Delta H_i]_{in}}. \quad (5)$$

Where, $W_{power\ block}$ is the calculated work extracted from power block, W_{pump} is the energy requirement of pumps, $W_{compressor}$ is the amount of work consumed by compressors including CO_2 and storage compressors. Likewise, Q_{loss} is an assumed heat loss to the environment, calculated as ~3% of the total energy balance of the plant [25].

5. Photovoltaic and wind energy profiles

To simulate the potential of the hybridisation of the proposed CLP process with renewable energy, a case study was analysed for renewable energy profiles from Whyalla, South Australia. Therefore, local data including average wind speed and daily solar radiation were obtained and used to model a network including wind turbine and photovoltaic solar farm coupled with the power grid. As can be seen in Fig. 4a, the monthly wind speed profile shows

that the average velocity changes from 6.05 m/s (the lowest in May) to 7.15 m/s (the highest in October). Therefore, it is anticipated that the wind turbine output will change ±16% across a year. Similarly, the intermittent behaviour of solar radiation reception shown in Fig. 4b can affect the performance of the photovoltaic panels resulting in variable output. While daily radiation varies from 2.49 kWh/m^2/day (the lowest in June) to 7.12 kWh/m^2/day (the highest in January), the output from the PV system can change ±63% across the year depending on the clearness index of the sky. Hence, to address the intermittent behaviour of wind and solar, in the proposed system, a battery storage unit was utilised to dampen the variation in renewable energy profiles.

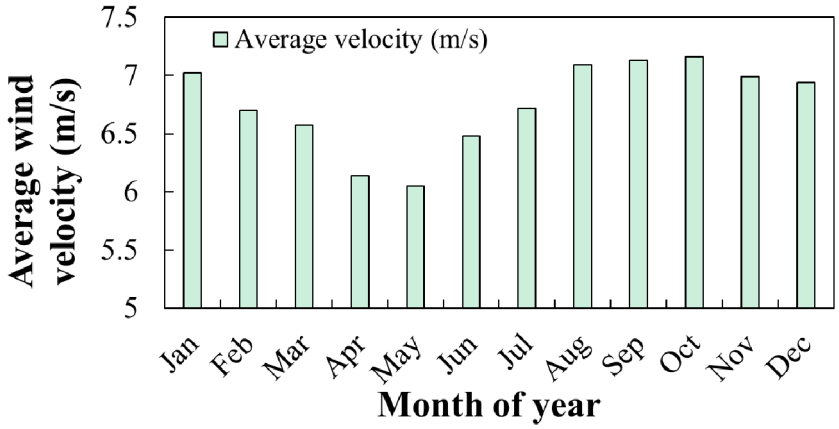

(a)

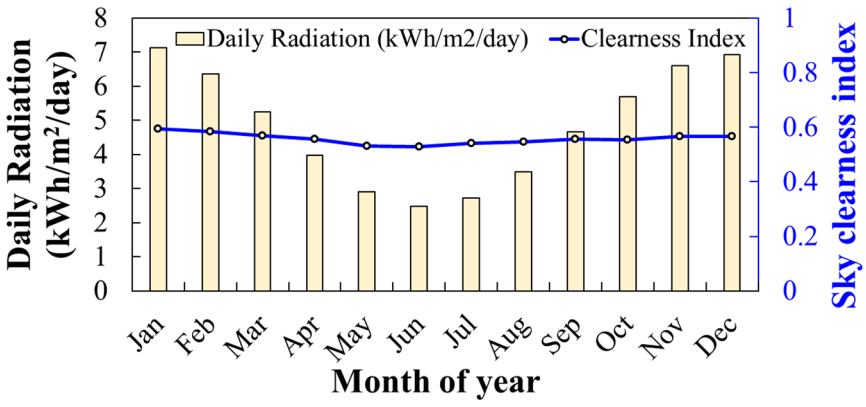

(b)

Fig. 4. (a) Monthly data for average wind speed in Whyalla, (b) monthly data used for daily solar radiation.

6. Results and discussion

In this section, the simulation results are presented in terms of thermodynamic parameters, chemical performance, and energy assessments of the reactors.

6.1.Effect of temperature on thermodynamic reaction performance

Synthetic Fuel Reactor (SFR): In the synthetic fuel reactor, two following reactions can potentially occur:

$$H_2O(g) + 2CO_2(g) + 2Cr(s) \rightarrow H_2(g) + 2CO(g) + Cr_2O_3(s), \quad \text{(R1)}$$

and,

$$H_2O(g) + 2CO(g) + 2Cr(s) \rightarrow H_2(g) + 2C + Cr_2O_3(s). \quad \text{(R2)}$$

In addition to the above reactions, a water gas shift reaction was included in the analysis because it can affect the content of CO_2 and H_2 in the reactor. Hence, thermochemical equilibrium analysis was performed to identify the dominant reaction in the reactor. The effect of temperature on the Gibbs free energy (ΔG), enthalpy of reaction (ΔH), and equilibrium constant of reaction for the SFR is presented in Fig. 5. A comparison of ΔG values of the two reactions (Fig. 5a) shows that reaction R2 exhibits $\Delta G > 0$ across all reactor temperatures. This means that it is not thermodynamically favourable, and the reaction will not proceed to equilibrium. Comparison of the enthalpy of both reactions (Fig. 5b) shows that only reaction R1 is exothermic (negative ΔH), while reaction R2 is endothermic, and hence it will produce solid carbon in the system leading to carbon deposition on chromium particles. Due to the positive Gibbs free energy and low equilibrium constant (Fig. 5c) for reaction R2, it is highly unlikely that this reaction will occur in the SFR and accordingly, the performance assessment of the SFR unit was based on reaction R1. Worth highlighting that ΔG and ΔH for reaction R1 show weak dependency on temperature (Fig.5a & Fig.5b), and hence (thermodynamically) this reaction can proceed at a wide range of reactor temperatures. However, the temperature of the SFR must be sufficiently high to offer reasonable Carnot efficiency, and high heat and mass transfer coefficient. Also, it is imperative to avoid a large temperature difference between the SFR and TPPR to avoid exergy loss due to the temperature difference. In the TPPR (thermal plasma reactor), the operating temperature can locally reach 5000 K. Hence, T=1273 K was chosen as a reference operating temperature for the SFR reactor to reduce the exergy destruction between the reactors. It is worth mentioning that this temperature can be achieved

using concentrated solar thermal energy or by burning renewable fuels such as biogas. However, assessing this is beyond the scope of the present research.

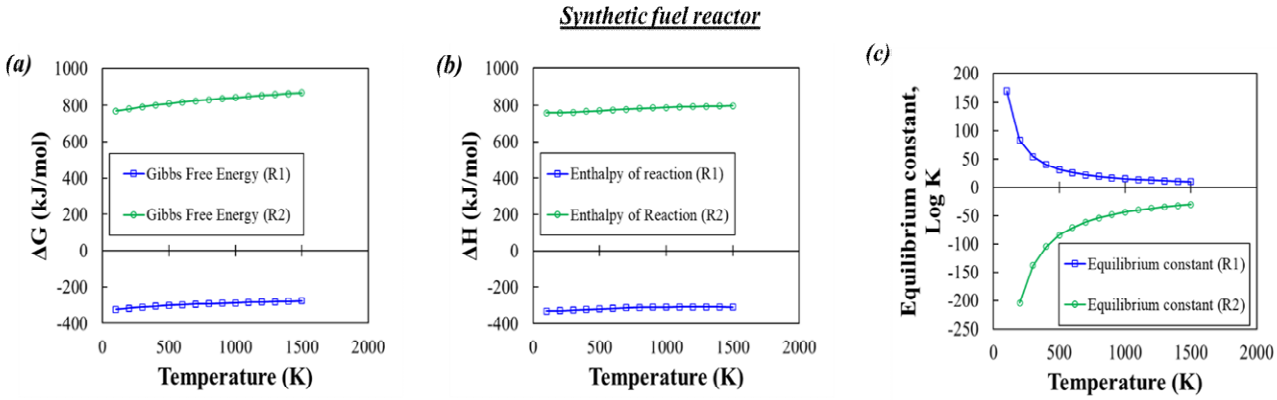

Fig. 5. The calculated dependence of; (a) Gibbs free energy, (b) enthalpy of reaction and (c) Equilibrium constant of the reactions on the temperature of the synthetic fuel reactor.

Thermal Plasma Particle Regenerator (TPPR): The localised temperature in the TPPR can reach several thousand degrees, which is suitable for driving reactions that have large positive Gibbs free energy.

The regeneration reaction in the thermal plasma is as follows;

$$Cr_2O_3(s) \rightarrow 2Cr(s) + 1.5O_2(g). \quad \text{(R3)}$$

As visualised in Fig. 6, there is a paradigm shift in the Gibbs free energy of the regeneration reaction (R3) at T=~4900 K as it becomes negative, meaning that reaction is spontaneous and will proceed towards the equilibrium point. At that temperature, the value equilibrium constant becomes positive (> 1) showing that the reaction will proceed to dissociate the chromium oxide to produce oxygen and chromium particles. The reaction is highly endothermic and requires 1100 kJ/mol energy to proceed towards equilibrium.

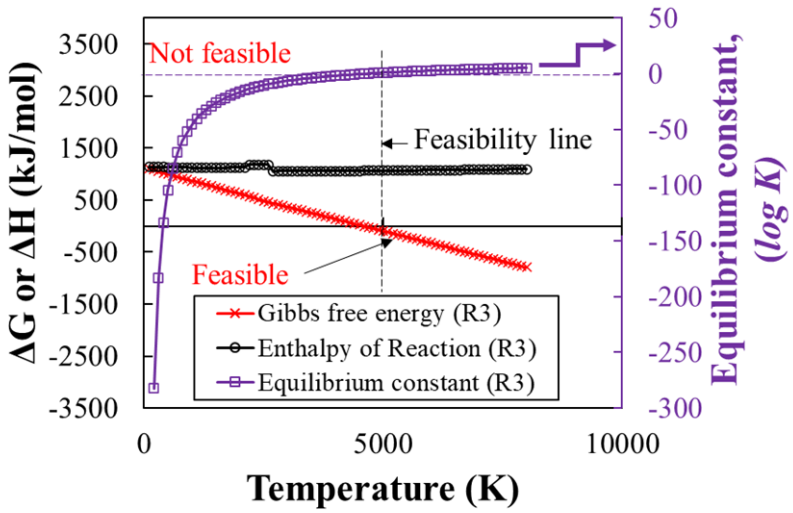

Fig. 6. The calculated Gibbs free energy, enthalpy of reaction and equilibrium constant of the particle re-generation reaction (R3) that convert Cr_2O_3 into Cr.

The thermal plasma reactor operates close to the equilibrium conditions thereby offering fast reactions with high chemical conversion extent.

6.2.Effect of CO_2/metal ratio

The molar fraction of CO_2 injected into SFR to circulate the metal particles between the reactors was identified as a key operating parameter affecting the performance of the reactor and the quality of the synthetic fuel. Fig. 7 shows the mole fraction of synthetic fuel composition against the molar CO_2/Cr ratio. The lowest mole fraction of CO_2 was observed at CO_2/Cr=0.5 in which the CO_2 is fully dissociated into synthetic fuel. However, for other ratios the amount of unreacted CO_2 in the synthetic fuel increases proportionally with the CO_2/Cr ratio, hence reducing the quality of the synthetic fuel. Interestingly, the hydrogen content is the highest at a molar ratio of CO_2/Cr ratio $\leq$ of 0.5. Overall, the highest synthetic fuel quality can be achieved within the range of $0.01 < CO_2/Cr < 0.5$. The mole fraction of CO initially increased reaching 0.47 at CO_2/Cr ratio=1 and then decreased to ~0.3 at CO_2/Cr ratio=4. Within the optimal range ($0.01 < CO_2/Cr < 0.5$) the CO mole fraction is between 0.2 and 0.3. It is worth mentioning that simulation showed that a minute amount of methanation occurred at CO_2/Cr ratio=0.5, however, the methane content is small (ppm-level) and can be ignored in further assessments.

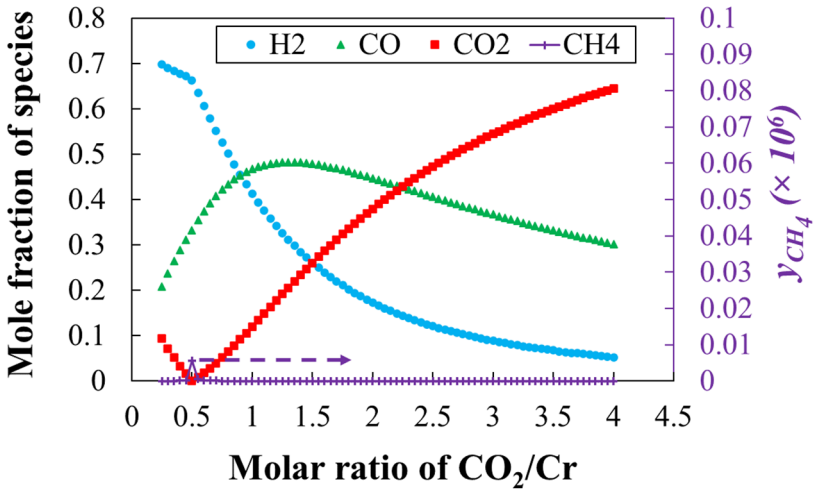

Fig. 7. Variation of mole fraction of species on the molar ratio of CO_2/Cr.

In Fig. 8, the variation of the molar ratio of H_2/CO and CO_2/CO with CO_2/Cr is represented. As can be seen, at CO_2/Cr ratio $\leq$ 0.5, the combustion quality approaches zero while the syngas quality (H_2/CO) is the highest. Likewise, with an increase in the molar ratio of CO_2/Cr, the value for syngas quality decreases. This is associated with the presence of unreacted CO_2 in the synthetic fuel together with complete oxidation of Cr particles which decreases the H_2 production. Interestingly, the dependence of the CO_2/CO molar ratio on CO_2/Cr shows a linear trend, while the reduction of the H_2/CO molar ratio is asymptotic (nonlinear). For industrial applications, a syngas quality >2.05 is generally considered a high-quality synthetic fuel that can be utilised in wide applications from Fischer-Tropsch to production of liquid fuel and fertilisers.

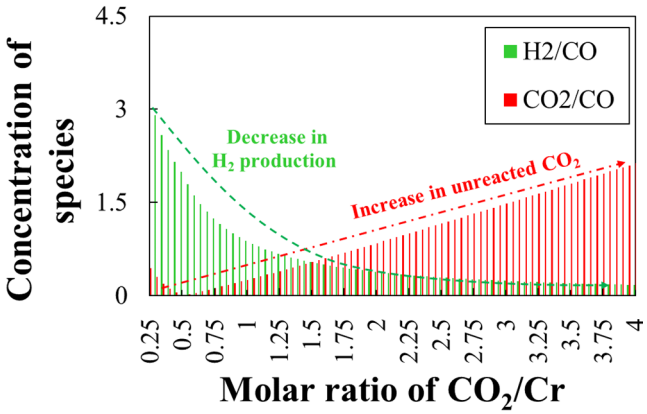

Fig. 8. Variation of the synthetic fuel production rate, combustion, and syngas quality indices with the molar ratio of CO_2/metal.

It was also identified that regulating the molar ratio of H_2O/Cr, at CO_2/Cr ratio ≤0.5, can increase the quality of the syngas by producing more hydrogen achieving the value of 2.05 and higher. This will be discussed in section 6.3.

6.3.Effect of steam/metal molar ratio

In Fig. 9, the dependence of the mole fraction of species in the syngas on steam/Cr is plotted at CO_2/Cr=1. At steam/Cr=1, the mole fraction of hydrogen is 0.41 which increased to 0.5 at steam/Cr=4. Interestingly, the mole fraction of CO_2 reached 0.1 at steam/Cr ratio=1 showing that this ratio is the optimum point in which hydrogen mole fraction is the highest, while the CO_2 mole fraction reaches its minimum value. The mole fraction of CO initially increased with an increase in steam/Cr and then reduced at steam/Cr ratio=0.85. As expected, no methanation occurred and the concentration of CH_4 remained within ppm-level.

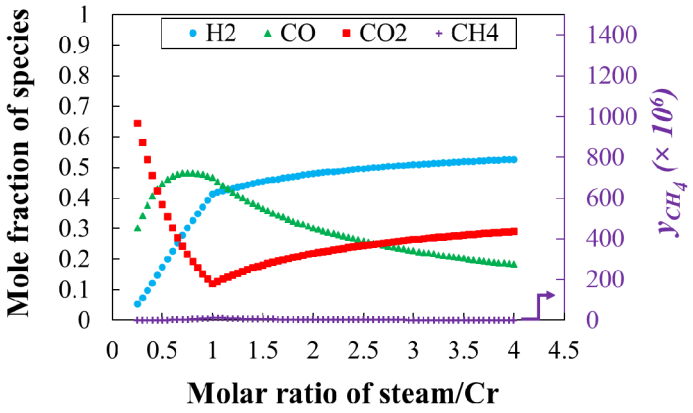

Fig. 9. Variation of mole fraction of species on the molar ratio of steam/metal.

The calculated dependence of syngas and combustion quality parameters on the molar ratio of steam/Cr is shown in Fig. 10. At the optimum ratio is steam/Cr=1, the combustion quality is low at 0.1 and the syngas quality is high at 1.35. However, a syngas quality of 1.5 is not suitable for processes such as liquid fuel production or Fischer-Tropsch processes. Producing syngas quality of 2.05 and higher requires a steam/Cr molar ratio of 2.8. This in turn increases the concentration of CO_2 to 0.25 and increases the combustion quality from 0.1 (at the optimum point) to 1.08. The unreacted CO_2 can be recycled using an amine absorption column. This, however, depends on end-user requirements, the threshold or acceptance level for CO_2, and the application of the synthetic fuel. Amine separation columns are energy-intensive and require a separate purification stage for amine once CO_2 is swept from syngas. Also, part of CO might

be absorbed by amine separators, which in turn increases the quality of the syngas. This, however, is beyond the scope of the present investigation.

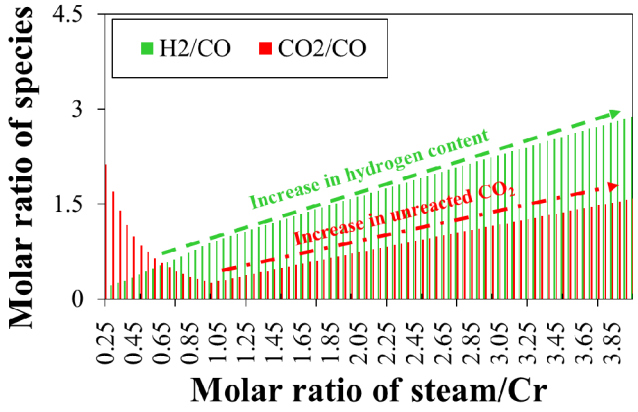

Fig. 10. Variation of the synthetic fuel production rate, combustion, and syngas quality indices (for steam/Cr ratio of 1).

Thermodynamic point for integration of renewable energy

For the proposed process, integrating renewable energy including solar photovoltaic electricity, and wind are an option for supplying the required energy for the thermal plasma reactor and auxiliary systems such as pumps and compressors. To integrate renewable energy, it is essential to identify optimum thermodynamic conditions for the operation of the process plant. As shown in Fig. 11, at steam/Cr ratio=2.8, CO_2/Cr=1.12 and T_{SFR}=1273 K and T_{TPPR}=5000 K, the highest calorific value (calculated with Eq. 2) and syngas quality ≥ 2.05 can be achieved.

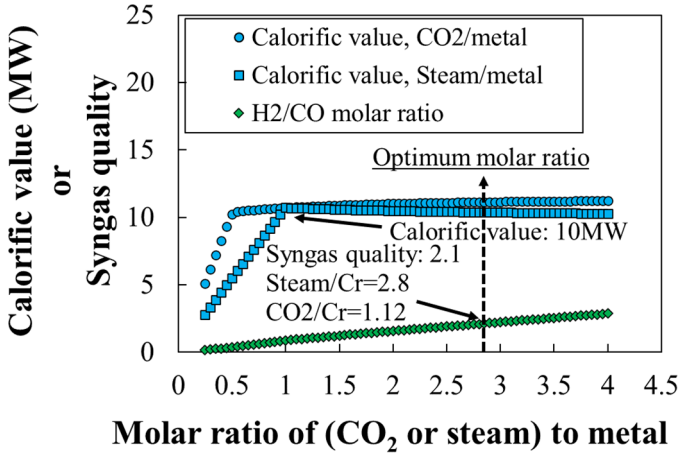

Fig. 11. Selection of the thermodynamic operating point(s) for operation and integration of the proposed plant with renewable energy.

6.4.Equilibrium chemical conversion

It is important to calculate the chemical conversion of the reactions occurring in SFR and TPPR at the identified optimum thermodynamic operating conditions (steam/Cr ratio=2.8, and CO_2/Cr=1.12, T_{SFR}=1273 K and T_{TPPR}=5000 K). As shown in Fig. 12, in the SFR, at temperature of ~1000 K, the chemical conversion extent reaches 99.5%. In the TPPR, due to the equilibrium operation of the reactor, at a temperature of ~4500 K, the reaction is initiated and quickly reach 95.5% completion, achieving a 100% conversion at T ≥ 5000 K. This is because the dissociation of chrome oxide is highly endothermic, and hence, increasing the temperature of the reactor promotes the chemical conversion of the reactor. Overall, the chemical conversion extent for both reactors is the highest at the optimum thermodynamic operating conditions.

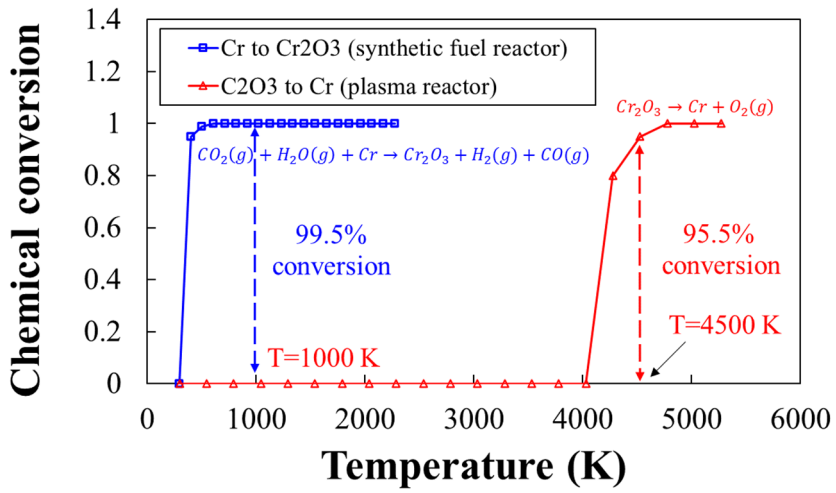

Fig. 12 Variation of the chemical conversion extent with temperature for both reactions in synthetic fuel and plasma reactors.

6.5.Thermodynamic energetic performance

Fig. 13, shows the plant energy efficiency, electricity generation and synthetic fuel quality as a comparison index (for SFR performance) against the temperature of both reactors. By increasing the temperature of the SFR, the efficiency of the plant slightly increases. For example, by increasing the temperature of SFR from 1273 K to 2273 K, the plant efficiency increases modestly from ~0.39 to ~0.43. However, this has resulted in a reduction in syngas quality from 2.1 to 1.03. This is because by increasing the temperature, less hydrogen is produced via the water gas shift reaction, thereby decreasing the syngas quality. However, increasing the temperature enhances the exergy that can be recovered in the form of sensible

heat via a heat recovery unit. This in turn increases the efficiency of the plant. Accordingly, the proposed process can be regulated depending on the end-user criteria and demands such as syngas quality, power production, and rate of CO_2 dissociation required. For the TPPR, the increase in the temperature of the reactor increases the energy demand.

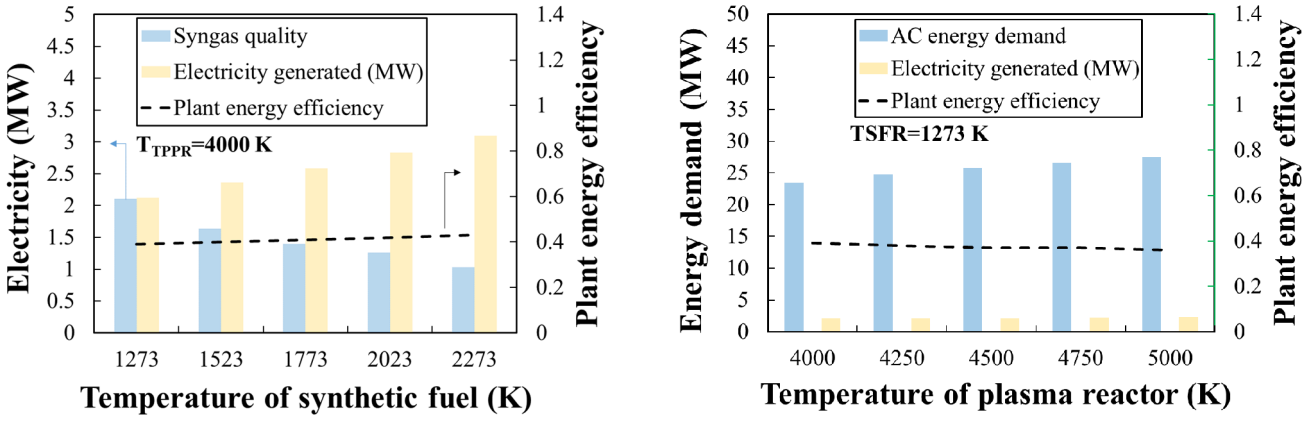

(a) (b)

Fig. 13. Effect of (a) temperature of synthetic reactor on syngas quality, electricity generation and energy efficiency of the plant, (b) temperature of plasma reactor on electricity demand of the plasma, plant electricity generation and energy efficiency of the plant.

While extra thermal energy is recovered by heat recovery, the efficiency of the plant decreases with an increase in the temperature of the plasma reactor. This is because the chemical conversion of the reactor increases such that more thermal energy is consumed to regenerate Cr particles in the thermal plasma reactor. For example, by increasing the temperature of the TPPR from 4000 K to 5000 K, the efficiency of the plant decreases modestly from 0.39 to 0.35. Hence, a trade-off trend is identified between the thermodynamic energy efficiency of the process plant and the exergy transported to the TPPR for dissociating Cr_2O_3.

6.6.Potential of the process for integration with renewable energy

In Fig. 14a, a schematic diagram of the energy network developed for the integration of renewable energy resources with the proposed system is shown. While the priority is set to use and increase the penetration of renewable energy (wind, photovoltaic or their blend), the power grid is utilized to compensate for any intermittent behaviour in renewable energy resources.

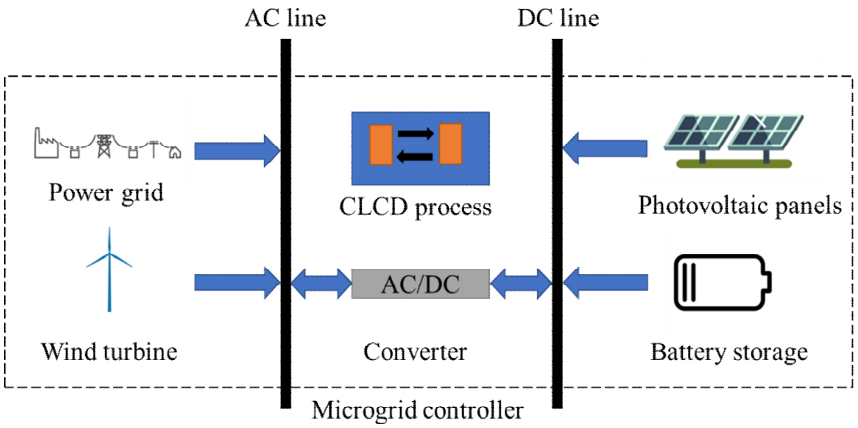

(a)

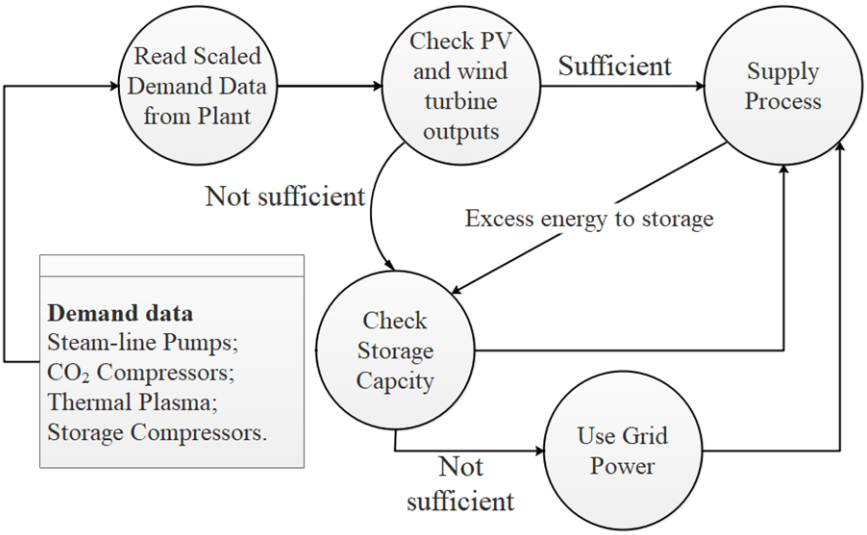

(b)

Fig. 14. (a) Schematic diagram of the proposed energy system developed for hybridisation of wind and solar with the proposed CLCD process, (b) The hybridisation logic used for utilisation of photovoltaic and wind energy for the proposed system.

The extra energy produced in peak hours is stored in a Li-ion battery to be utilized for shortage periods when there is no renewable energy available. Hence, the power grid was the least option to be used for meeting the process demand. Notably, wind turbines and power from the grid produce electricity in AC form, while energy extracted from battery units and photovoltaic panels are in DC form, thereby, requiring a smart AC/DC converter to reshape DC electricity to AC form to be injected into the process. The decision-making flow chart given in Fig. 14b shows how the microgrid controller utilizes renewable energy resources. Initially, the availability of the energy is checked by the controller to check if the demand of the process can be met either with photovoltaic energy or wind. If the energy flow in the system is not

sufficient, the battery storage is checked. If demand can still be met with the energy stored in the battery, then the controller will connect the battery to the system, while estimating the potential of the battery for the next operating hour. If it cannot meet the demand, then, the power grid is gradually ramped up until renewable energy is back to the energy flow of the system. The hourly and monthly energy demand of the proposed process (mainly from the thermal plasma reactor) is shown in Figs 15 (a-c). As can be seen, in Fig. 15a, the hourly data shows that the energy demand of the process fluctuates around the average demand value of 25 MW. Also, as represented in Fig. 15b, the monthly energy demand varies between 22 MW and 29 MW across the year. It was assumed that the process operates continuously with full capacity without any overhaul during the calculated operation year. The hourly-monthly variation of the process demand can be found in form of a scaled contour given in Fig. 15c.

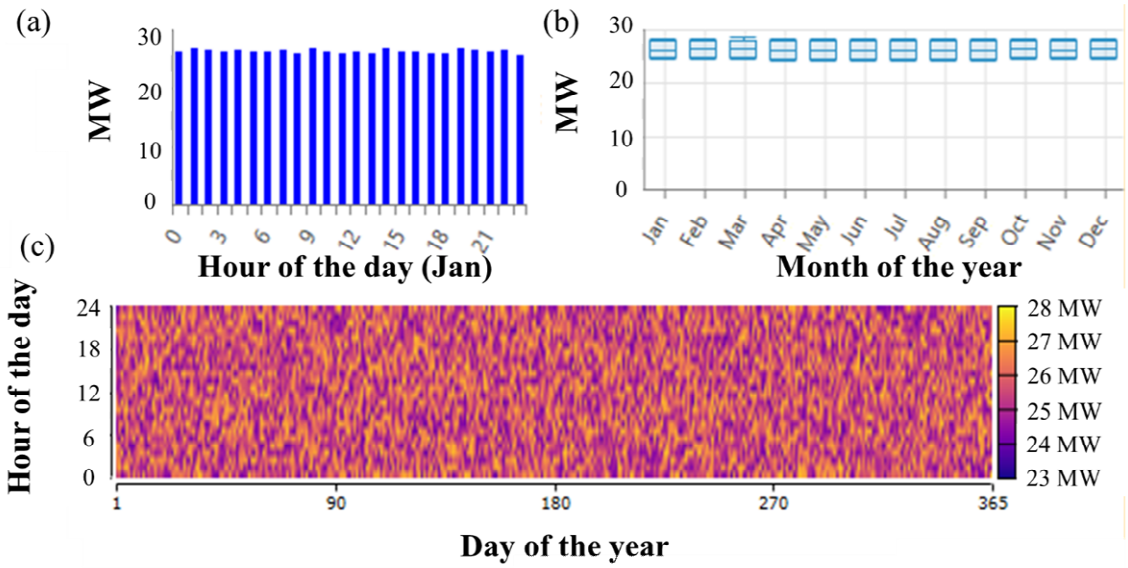

Fig. 15. (a) Hourly and monthly energy demand profile of the proposed system used in the hybridisation simulations.

The results of energy analysis showed that:

(1) The proposed process has sufficient resilience against integration with renewable energy resources providing that the integrated process is backed by an energy storage unit.

(2) A trade-off trend was identified between the renewable energy share (RES), size of the battery storage, and the capacity of photovoltaic panels and the number of wind turbines. As shown in Fig. 16, for the case without an energy storage unit, for PV capacity up to 20 MW, and wind turbine capacity up to 15 MW, less than 8% of the process demand can be supplied

with renewable energy. However, for a process integrated with 20 MWh energy storage, the blue region becomes smaller (7.5 MW for wind turbines and 10-20 MW for photovoltaic solar). This means that a smaller number of wind turbines and PV panels are required to be installed. By increasing the capacity of the energy storage unit, the fraction of renewable energy share increases reaching the storage capacity of 40 MWh in which renewable energy share becomes independent from battery storage. For example, for two configurations with battery storage of 100 MWh and 200 MWh, the renewable energy share remains the same. This is because enlarging the battery size is not useful as long as renewable energy is not sufficient to meet the process demand and also contribute to the battery charging cycle.

(3) The maximum renewable energy share of > 64% was calculated for the LCLD process hybridised with wind and photovoltaic solar with battery storage of 40 MWh, PV capacity of 30 MW and wind turbine installation capacity of 22.5 MW. Overall, the capacity of the energy storage unit is the key to determining the renewable energy fraction in the system. Thus, to integrate the proposed system, it is recommended to consider the end-user requirements, the area available for installation of the storage unit, the efficiency of the wind turbine, photovoltaic panels. A robust techno-economic analysis can further justify the accurate capacity for production and storage units.

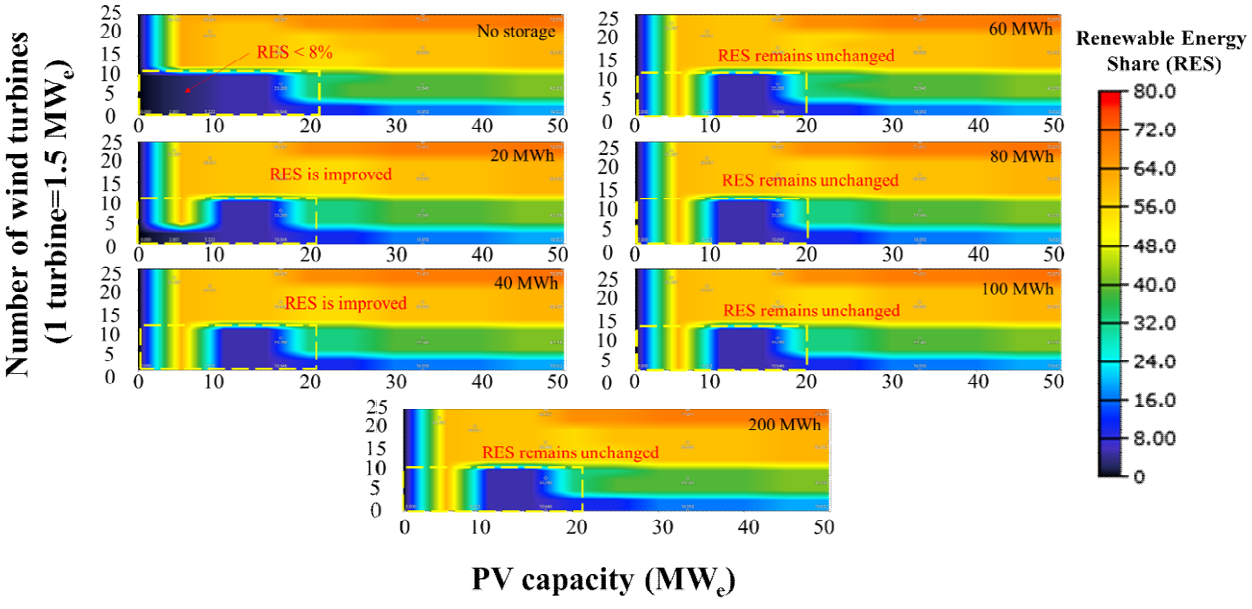

Fig. 16. Effect of battery storage, PV and wind turbine capacities on the calculated renewable energy solar fraction.

7. Conclusion

References

[1] R. Rapier, Fossil Fuels Still Supply 84 Percent Of World Energy—And Other Eye Openers From BP's Annual Review, June, 2020.
[2] R. York, Do alternative energy sources displace fossil fuels?, Nature Climate Change, 2 (2012) 441-443.
[3] S.A. Morrissey, J.P. Reser, Natural disasters, climate change and mental health considerations for rural Australia, Australian Journal of Rural Health, 15 (2007) 120-125.
[4] I.P.O.C. Change, Climate change: The IPCC scientific assessment, Mass, Cambridge, (1990).
[5] S.N. Seo, Beyond the Paris Agreement: Climate change policy negotiations and future directions, Regional Science Policy & Practice, 9 (2017) 121-140.
[6] Ş. Kılkış, G. Krajačić, N. Duić, M.A. Rosen, M.d. Ahmad Al-Nimr, Accelerating mitigation of climate change with sustainable development of energy, water and environment systems, Energy Conversion and Management, 245 (2021) 114606.
[7] M.F. Demirbas, M. Balat, Recent advances on the production and utilization trends of bio-fuels: A global perspective, Energy Conversion and Management, 47 (2006) 2371-2381.
[8] W. Gu, T. Ma, S. Ahmed, Y. Zhang, J. Peng, A comprehensive review and outlook of bifacial photovoltaic (bPV) technology, Energy Conversion and Management, 223 (2020) 113283.
[9] NREL., Electricity Annual Technology Baseline (ATB) Data, USA, 2021.
[10] A.L. Rispoli, G. Iaquaniello, A. Salladini, N. Verdone, M.R. Pepe, A. Borgogna, G. Vilardi, Simultaneous decarbonisation of steel and Oil&Gas industry by MSW gasification: Economic and environmental analysis, Energy Conversion and Management, 245 (2021) 114577.
[11] I. Deniz, F. Vardar-Sukan, M. Yüksel, M. Saglam, L. Ballice, O. Yesil-Celiktas, Hydrogen production from marine biomass by hydrothermal gasification, Energy Conversion and Management, 96 (2015) 124-130.
[12] H.-W. Wu, T.-T. Hsu, C.-M. Fan, P.-H. He, Reduction of smoke, PM2.5, and NOX of a diesel engine integrated with methanol steam reformer recovering waste heat and cooled EGR, Energy Conversion and Management, 172 (2018) 567-578.
[13] C. Luo, B. Dou, H. Zhang, D. Liu, L. Zhao, H. Chen, Y. Xu, Co-production of hydrogen and syngas from chemical looping water splitting coupled with decomposition of glycerol using Fe-Ce-Ni based oxygen carriers, Energy Conversion and Management, 238 (2021) 114166.
[14] W. Ma, C. Chu, P. Wang, Z. Guo, B. Liu, G. Chen, Characterization of tar evolution during DC thermal plasma steam gasification from biomass and plastic mixtures: Parametric optimization via response surface methodology, Energy Conversion and Management, 225 (2020) 113407.

[15] H. Qi, P. Cui, Z. Liu, Z. Xu, D. Yao, Y. Wang, Z. Zhu, S. Yang, Conceptual design and comprehensive analysis for novel municipal sludge gasification-based hydrogen production via plasma gasifier, Energy Conversion and Management, 245 (2021) 114635.
[16] N.D. Montiel-Bohórquez, A.F. Agudelo, J.F. Pérez, Effect of origin and production rate of MSW on the exergoeconomic performance of an integrated plasma gasification combined cycle power plant, Energy Conversion and Management, 238 (2021) 114138.
[17] D. Li, V. Rohani, F. Fabry, A.P. Ramaswamy, M. Sennour, L. Fulcheri, Experimental study on plasma-catalytic synthesis of hydrocarbons from syngas, Applied Catalysis A: General, 588 (2019) 117269.
[18] J. Gonzalez-Aguilar, M. Moreno, L. Fulcheri, Carbon nanostructures production by gas-phase plasma processes at atmospheric pressure, Journal of Physics D: Applied Physics, 40 (2007) 2361.
[19] R.E. Haufler, J. Conceicao, L.P.F. Chibante, Y. Chai, N.E. Byrne, S. Flanagan, M.M. Haley, S.C. O'Brien, C. Pan, Efficient production of C60 (buckminsterfullerene), C60H36, and the solvated buckide ion, Journal of Physical Chemistry, 94 (1990) 8634-8636.
[20] D.H. Parker, P. Wurz, K. Chatterjee, K.R. Lykke, J.E. Hunt, M.J. Pellin, J.C. Hemminger, D.M. Gruen, L.M. Stock, High-yield synthesis, separation, and mass-spectrometric characterization of fullerenes C60 to C266, Journal of the American Chemical Society, 113 (1991) 7499-7503.
[21] V. Rohani, S. Takali, G. Gérard, F. Fabry, F. Cauneau, L. Fulcheri, A new plasma electro-burner concept for biomass and waste combustion, Waste and Biomass Valorization, 8 (2017) 2791-2805.
[22] H. Huang, L. Tang, Treatment of organic waste using thermal plasma pyrolysis technology, Energy Conversion and Management, 48 (2007) 1331-1337.
[23] H.A. Kazem, J.H. Yousif, Comparison of prediction methods of photovoltaic power system production using a measured dataset, Energy Conversion and Management, 148 (2017) 1070-1081.
[24] J. Feng, W.Z. Shen, Wind farm power production in the changing wind: Robustness quantification and layout optimization, Energy Conversion and Management, 148 (2017) 905-914.
[25] J.S. Goodling, Microchannel heat exchangers: A review, International Society for Optics and Photonics, pp. 66-83.